Quarterly Reviews of Biophysics

cambridge.org/qrb

Where in the cell is my protein?

David J. DeRosier

Brandeis University, Waltham, MA, USA

Abstract

The application of cryo-correlative light and cryo-electron microscopy (cryo-CLEM) gives us a way to locate structures of interest in the electron microscope. In brief, the structures of interest are fluorescently tagged, and images from the cryo-fluorescent microscope (cryo-FM) maps are superimposed on those from the cryo-electron microscope (cryo-EM). By enhancing cryo-FM to include single-molecule localization microscopy (SMLM), we can achieve much better localization. The introduction of cryo-SMLM increased the yield of photons from fluorophores, which can benefit localization efforts. Dahlberg and Moerner (2021, Annual Review of Physical Chemistry, **72**, 253–278) have a recent broad and elegant review of super-resolution cryo-CLEM. This paper focuses on cryo(F)PALM/STORM for the cryo-electron tomography community. I explore the current challenges to increase the accuracy of localization by SMLM and the mapping of those positions onto cryo-EM images and maps. There is much to consider: we need to know if the excitation of fluorophores damages the structures we seek to visualize. We need to determine if higher numerical aperture (NA) objectives, which add complexity to image analysis but increase resolution and the efficiency of photon collection, are better than lower NA objectives, which pose fewer problems. We need to figure out the best way to determine the axial position of fluorophores. We need to have better ways of aligning maps determined by FM with those determined by EM. We need to improve the instrumentation to be easier to use, more accurate, and ice-contamination free. The bottom line is that we have more work to do.

Review

Cite this article: DeRosier DJ (2021). Where in the cell is my protein? *Quarterly Reviews of Biophysics* **54**, e9, 1–12. https://doi.org/10.1017/S003358352100007X

Received: 25 January 2021
Revised: 13 June 2021
Accepted: 17 June 2021

Key words:
Cryo-CLEM; cryo-electron microscopy; cryo-ET; cryo-superresolution fluorescence microscopy; FIB-SEM microscopy; localization of structures

Author for correspondence:
David J. DeRosier,
E-mail: derosier@brandeis.edu

Table of contents

Introduction

Structural cell biology aims to visualize the distribution of matter in cells and subcellular structures and to determine which features correspond to which molecules or even which subdomains. In the distant past, cells were fixed, stained, and sectioned in order to see their interior features by electron microscopy. We could sometimes tell very generally where in the cell our molecules of interest were located, but the molecular details were not well preserved during the preparation. The introduction of frozen-hydrated cryo-electron microscopy (cryo-EM)

CAMBRIDGE UNIVERSITY PRESS

(Adrian *et al.*, 1984) meant that biological structures could be preserved in an essentially native state. By fast freezing hydrated EM grids, water was prevented from crystallizing. It was as if all the atoms were frozen in their tracks. That is not strictly true, but there is now much evidence that this method preserves biological structures to atomic detail.

With the addition of improved microscopes, cameras, and image-processing programs came the resolution revolution in cryo-EM (Kühlbrandt, 2014) and the cryo-electron tomography (cryo-ET) of frozen-hydrated specimens (Baumeister *et al.*, 1999). Now we can do much better. Cryo-ET of frozen-hydrated specimens can display in three-dimensions (3D) the interiors of large machines, organelles, and cells in their near native states and in exquisite, near atomic detail (e.g. Metlagel *et al.*, 2019; Schur, 2019: Chakraborty *et al.*, 2020; Ke *et al.*, 2020, Watanabe *et al.*, 2020). We wish to consider the ways in which we can locate a molecule or a part of a molecule, which we will call the target, in a 3D cryo-ET map.

If the interesting part of the cell is thin enough (say <500 nm), we can generate tomograms directly from the cells on the EM grid. Most cells, however, are too thick for imaging their interiors by cryo-EM. One particularly productive avenue of viewing the interiors of thick cells by cryo-ET is the use of focused ion beam (FIB) milling to generate thin lamellae cut through cells (Marko *et al.*, 2006, 2007; Rigort and Plitzko, 2015). The question is, where do we mill the lamella so that it contains our target structure? In some cases, it may not matter because structures of interest are easily found in most lamellae, but we still must find the target structure somewhere in the 3D tomogram. If we are lucky, the target may be located either because its structure is known and it is of sufficient size and shape to be picked out by cross-correlation (Bohm *et al.*, 2000; Rickgauer *et al.*, 2017), or because the target is associated with a known structure that is identifiable (Watanabe *et al.*, 2020). When those lucky situations do not apply, we would like, in the first place, to know where to mill our lamellae. At present, we can generate perhaps ~20 lamellae on a single grid (Buckley *et al.*, 2020, Zachs *et al.*, 2020) but that effort takes a big part of a day. Because generating cryo-ETs from lamellae can take hours of expensive EM time and can generate around a terabyte of data, we would like to be sure we have a good chance of finding our target in the resulting tomogram. In the second place, we need to locate our target within the tomogram.

What avenues are available to us?

We could use a fluorescent microscope (FM) to locate the general volume of our target. Given the use of frozen-hydrated samples for EM, it made sense to carry out FM on the very same frozen samples being imaged in the EM. Thus, was cryo-correlative light and cryo-electron microscopy (cryo-CLEM) introduced in 2007 (Sartori *et al.*, 2007; Schwartz *et al.*, 2007). The goal is to use cryo-CLEM to increase the probability of seeing our targets in the EM. Moreover, we may want to freeze/trap a cell at some particular stage, and having marked the structure of interest with a fluorescent tag, we will know where to look for our target in the cryo-ET. But the resolution of FM images, being about 250 nm laterally and 500 nm axially, is not accurate enough either to determine where to mill a 150 nm thick lamella that contains our target or to locate our target in the tomogram

SMLM methods achieve better localization than plain FM.

Single-molecule localization microscopy (SMLM) such as STORM (Rust *et al.*, 2006) or (F)PALM (Betzig *et al.*, 2006; Hess *et al.*, 2006) provides a way of localizing fluorescent tags more precisely than expected from the resolution of the FM (see Box 1). There are many ways to put a fluorescent tag on a target molecule either by cloning the gene for a suitable fluorescent protein (FP) into the gene of the target molecule (e.g. Liu *et al.*, 2015) or by binding an appropriate fluorescent dye to the target (e.g. Bates *et al.*, 2012).

Because we can choose the photophysical properties of the SMLM fluorophores, we can arrange that only a few of the fluorophores are fluorescing at any one time. The positions of these few fluorescing tags can be determined by fitting the point spread function (PSF) to the observed distribution of photons and thus localize the tag to a fraction of the PSF. When these fluorescing tags switch off, a few more tags, when turned on, can be mapped until they switch off. This process is then repeated until all the fluorophores within the entire field of view are precisely mapped. In this way, we eliminate the problem of overlap of fluorescing tags in space by separating them in time. The equation governing the error in position is given and discussed in Box 1. The take home message is that the precision of localization is much, much better than the Rayleigh resolution, that the more fluorescent photons captured the smaller the error, and that the higher the number of background photons the bigger the error.

What we really want to know, however, is the accuracy of the localization, which may differ from the precision due to other sources of error such as deviation of the PSF from a Gaussian distribution or from errors in the registration of the SMLM image and the tomogram. Thus, in our mind, we need to keep separate errors in precision from errors in accuracy from errors in registration.

Other factors also contribute to an increase in errors. If the fluorophore is out of focus, the observed PSF in the image and the error will be larger. The mechanical stability of the microscope can also contribute to the observed PSF. Contributors include vibration, which can come from sound in the room as well as from the platform on which the microscope sits, and thermal drift. Moreover, not all objectives perform to the theoretically calculated PSF. One solution is to determine experimentally the PSF, which is a good check on how well a setup is performing. Determination of the PSF is easily done with fluorescent nanobeads, which are available commercially.

The errors discussed above are those for the precision of the location of the fluorophore, whereas the accuracy is determined by how close the estimated position is to the true position of the fluorophore. The formula given in Box 1 assumes that the distribution of photons in the PSF is Gaussian, which is an approximation. The approximation is good if the fluorophores are freely tumbling, but a correct description of the distribution of photons in the PSF derives from the predicted radiation from a molecular dipole (Mortensen *et al.*, 2010). We will return to this point later.

For a particular fluorophore, we also want to know the predicted best resolution we can achieve. This will depend on the photophysical properties of the fluorophore. Pennacchietti *et al.* (2017) have made a detailed study of a Dendra2. In selecting a fluorophore to use under cryo-FM, we could use their methodology as a model for evaluating candidate fluorophores.

https://doi.org/10.1017/S003358352100007X Published online by Cambridge University Press

Box 1.

The formula for resolution in the light microscope according to the Rayleigh criterion is given by

$$x = 0.61\,\lambda n/\mathrm{NA}$$

where x is the resolution (nm), λ is the wavelength (nm), n is the refractive index of the sample, and NA is the numerical aperture of the objective lens. If, for example, $\lambda = 400$ nm, $n = 1.5$, and NA = 1.45, then our resolution is $x = 252$ nm. In contrast to the Rayleigh resolution, SMLM resolution is derived from the precision or standard error of the mean of the localization as given in the equation below:

$$\langle(\Delta x)^2\rangle = \frac{s^2}{N} + \frac{a^2}{12N} + \frac{4\sqrt{\pi}s^3b^2}{aN^2}$$

where Δx is the standard error of the mean position of the distribution of observed photons, s is the standard deviation (nm) of a Gaussian distribution, which is a simple model for the PSF, N is the number of photons collected in the peak, a is the pixel size (nm), and b is the background photons per pixel (Thompson *et al*., 2002). The idea is that the fluorophore's position is within $2 \times \Delta x$ of the location of the peak intensity with a 95% probability. An improved version of the equation has been given by Mortensen *et al*. (2010), but the equation above captures the essence of determining the error of localization. Ignoring the last two terms for a moment, we see that the error depends only on the 'width' of the PSF and the number of photons. Thus, we can reduce the error by decreasing the width of the PSF, increasing the number of photons, or both. As an example, if we collect 500 photons, we improve the rms error by a factor of $500^{1/2} = 22$ compared to the Rayleigh resolution of an FM. But a high background can significantly change our final resolution. If s is ∼230 nm, N is 500 photons, a is ∼140 nm, and $b = 0$, we would have an rms error of 10 nm. The second term of the equation, which is due to pixelation of the image, only increases the error estimate by 0.2 nm in our example. Turning to the third term, which is due to background, we find that a 1% background count ($b = 5$) would increase the error estimate from 10 to 13 nm while a 5% background count ($b = 25$) gives an error estimate of 40 nm, a 400% increase. Thus, the background can be an important contributor to the error. Typically, observed errors are 20–50 nm (Li and Vaughan, 2018). The key point is that the errors in localizing the tag are much smaller in SMLMs than the classical resolving power of the FM.

The determination of *z*, the depth of the fluorophore, is trickier than that of *x* and *y*.

The error in z follows the same equation as those for x and y, except that we need to know the PSF in the z direction. One method is to take a through focal series and carry out the fitting in 3D instead of two-dimensional (2D). Another method is to introduce astigmatism (Kao and Verkman, 1994), which obviates the need to obtain a through focal series. Either a cylindrical lens or an adaptive optics lens (Siemons *et al*., 2020) can introduce astigmatism, which causes the PSF to elongate laterally in one direction if the fluorophore is above the plane of focus and at right angles to that if it is below (Fig. 1*a*). A series of through focal images of fluorophores on a flat surface can be used to generate a calibration curve of the x and y widths of the PSF as a function of defocus (i.e. z; Fig. 1*b*). The curves can then be used to determine the z positions of the fluorophores (Huang *et al*., 2008, Chien *et al*., 2015). In a STORM experiment using CY3 and Alexa 647 and within about 100 nm of focus, errors were about 10 nm in x and y and about 20–35 nm in z (Huang *et al*., 2008). It is important to note that the error in localization increases as the amount of underfocus or overfocus increases. This level of error suggests that the use of astigmatism is a feasible way of determining the z position of a tag under the right circumstances – more later. There are other methods of determining z as well: for example, the biplane method (Juette *et al*., 2008) or the double-helix PSF (Lew *et al*., 2010). These two may perform better than the method using astigmatism, but they require more modifications to the optics.

These results were all obtained at ambient temperature. The thrust of this paper is to adapt SMLM methods for cryo-conditions, which is the forefront of CLEM. Thus, we need cryo stages and cryo-fluorophores.

There are existing cryo-stages compatible with objectives of different numerical apertures.

A schematic of a cryo-SMLM is shown in Fig. 2. There are a range of different realizations of cryo-LM stages for such a cryo-FM, some of which are available commercially. In one design (Fig. 3*a*), the cold samples are viewed with air or vacuum coupled objectives (e.g. Sartori *et al*., 2007, Schwartz *et al*., 2007, Weisenburger *et al*., 2017). Linkam Scientific Instruments offers the CMS196 cold stage, which can be added to a fluorescence microscope, and Leica Microsystems offers the Thunder Imager EM cryo-CLEM microscope, which has the cold stage (see Schorb *et al*., 2017) as an integral part of the microscope. The designs for the two commercial instruments are a bit different from that in Fig. 3*a* in that the sample is held by a horizontal arm, which additionally permits transmitted light. Instead of the coverslip, the front surface of the objective is in contact with the cold gas. The important point is that all the objectives are air or vacuum coupled and can be operated essentially at ambient temperature.

The air or vacuum coupling, however, restricts the numerical aperture (NA) to <1. The NA may also be limited to still lower values if a long working distance between sample and objective is required. The NA derives from the angular width of the cone of light that enters the objective: the larger the NA, the wider the angle. The NA, therefore, influences the resolution of the resulting image in two ways. First, the dimension of the PSF is proportional to the inverse of the NA. Hence, a higher NA means a smaller PSF. Second, the number of photons captured is roughly proportional to NA squared. Thus, if we increase the NA of the objective, we decrease root mean squared error by a factor of $\sim 1/\mathrm{NA}^2$. Can a higher NA objective improve localization of the fluorophore under cryogenic conditions?

Several groups have built cryo-microscopes that employ immersion lenses having an NA of 1.2–2.17. An NA of 1.2 compared to an air-coupled objective with an NA of, say, 0.8 would decrease the error by a factor of about 2, i.e. $(1.2/0.8)^2$. In one version of a cryo-microscope, the 1.3 NA objective itself operates at cryo temperatures (Fig. 3*b*). The objective is optically coupled to the sample by liquid propane (Le Gros *et al*., 2009). One advantage of this design is that the plunge freezer is built into the cryo-stage in which the room temperature, blotted sample is plunged

https://doi.org/10.1017/S003358352100007X Published online by Cambridge University Press

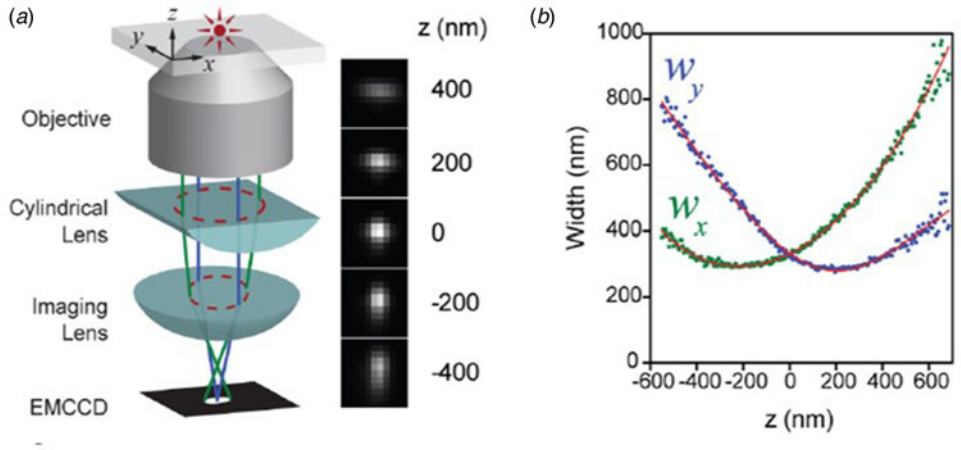

Fig. 1. (*a*) Schematic diagram showing the insertion of a cylindrical lens in the optical path in an inverted microscope. The cylindrical lens introduces astigmatism into the PSF as seen in the through focus series of images to the right of the schematic drawing. At −400 nm, the PSF is elongated vertically in the image while at +400, it is elongated horizontally. (*b*) Plots of the horizontal width and vertical width *versus* distance from focus. The w_x and w_y widths of fluorophores in an image can be used to determine their *z* positions relative to the plane of focus. Reprinted from Fig. 1 by permission from © American Association for the Advancement of Science, *Science*, Huang *et al.* (2008).

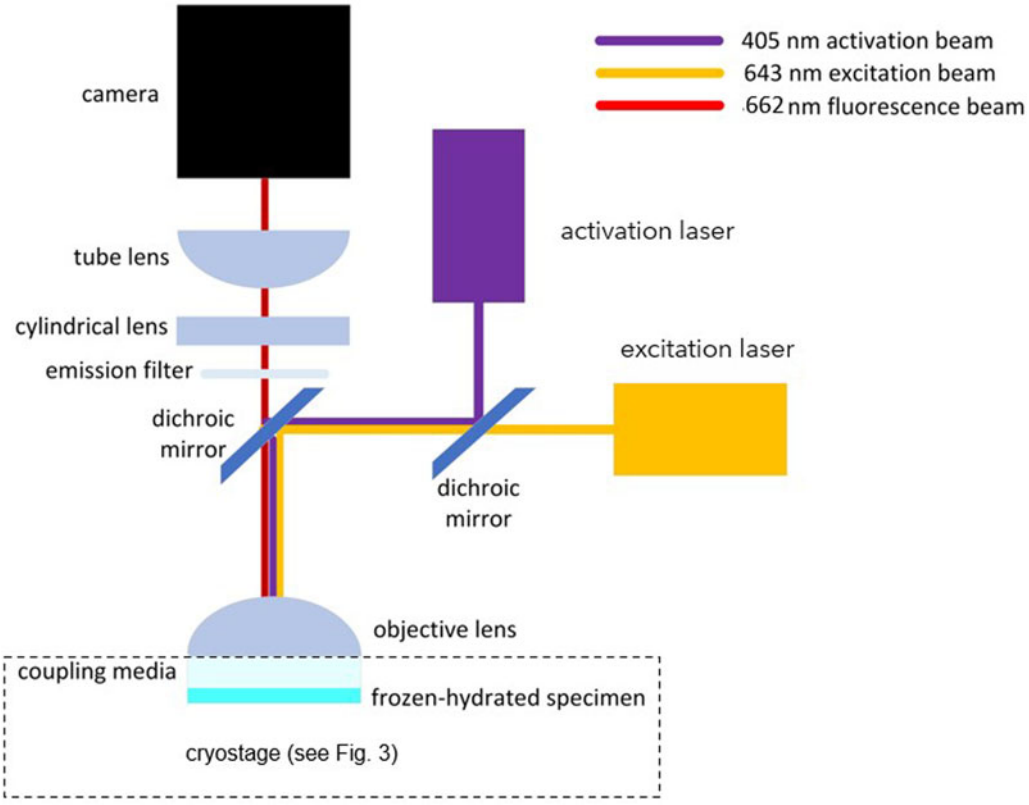

Fig. 2. Schematic of a cryo-fluorescence microscope that can be used for SMLM. The 405 nm laser is typically used to switch fluorophores such as PSmOrange from orange to red. The 643 nm laser excites the switched PSmOrange fluorophore, which emits at 662 nm. The dichroic mirror to the left of the lasers transmits the excitation beam and reflects the activation beam making the two beams collinear. The other dichroic mirror reflects the laser beams onto the sample via the objective lens while transmitting the fluorescence beam returning from the sample. The returning beam is further isolated from the activation and excitation beams by the emission filter. From there the fluorescence beam is made stigmatic by a cylindrical lens, focused by the tube lens, and recorded by the camera. Additional lasers can be added using suitably chosen dichroic mirrors to merge the beams. To reflect these additional beams onto the sample and permit passage of the emitted fluorescent beam, we need to switch the second dichroic mirror and the emission filter to work with the altered wavelengths. The frozen-hydrated sample is kept frozen either by a cryo-block or by cold gas or liquid around the sample as indicated in one of the cryo-stage designs in Fig. 3.

into the liquid propane filled viewing chamber of the microscope. A drawback of this design is that the cold stage cannot be attached to a standard FM.

The other two designs, which are both described in Fig. 3*c*, have ~1.2 NA objectives that operate at or near ambient temperature (Nahmani *et al.*, 2017; Faoro *et al.*, 2018). The objective lens

https://doi.org/10.1017/S003358352100007X Published online by Cambridge University Press

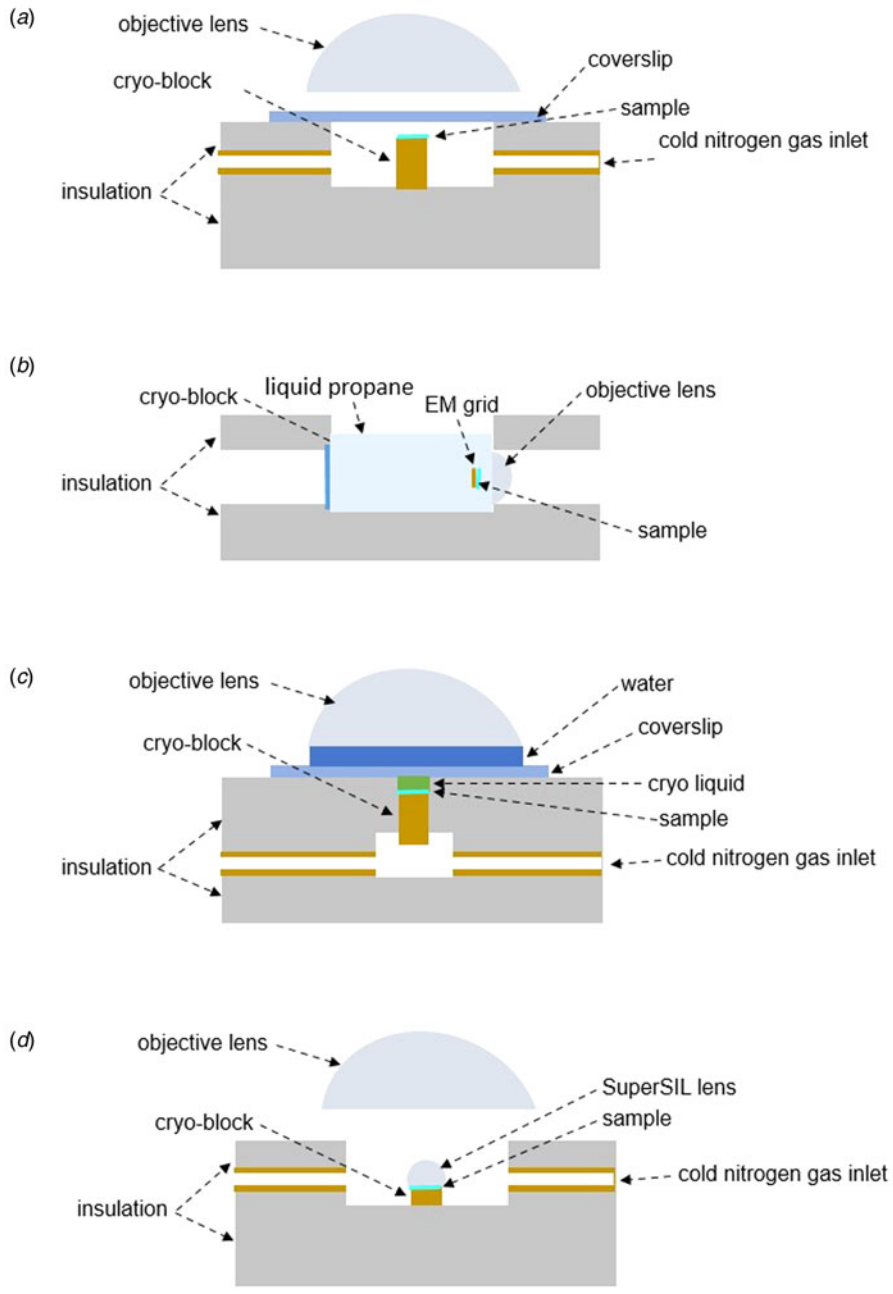

Fig. 3. Schematics of four cold stage designs. (*a*) Cold nitrogen gas flows past the cryo-block, which holds the sample. A coverslip separates the cold sample from the objective lens. The objectives are limited to NAs <1. (*b*) In this design, a grid has been plunged and held in place by tweezers (not shown). The optical track runs horizontally from left to right passing through a window, the liquid propane, the sample, and then to the objective lens and camera (not shown). The liquid propane is maintained at the proper temperature by liquid nitrogen (not shown). The objective can have an NA of 1.3. (*c*) Cold nitrogen gas maintains vitreous nature of the ice in the sample. To permit the use of higher NAs, e.g. NA = 1.2, the sample and objective are optically coupled by a cryo-fluid, coverslip, and water. The cold stage operates at steady state. Heat, supplied to the water layer by some mechanism (not shown), is conducted through the coverslip and cryo-liquid to the sample. The heat is carried away by cold-nitrogen-gas cooled cryo-block on which the sample sits. The heat conductances of the coupling layers are such that the specimen is kept below the transition temperature of vitreous ice. (*d*) Cold nitrogen gas keeps the sample below the vitreous ice transition temperature. The sample sits under a high NA superSIL lens, which serves as the objective. Below the sample lies the virtual image of the sample made by the superSIL lens. The virtual image is reimaged by a second, longer-working- distance objective, which operates at ambient temperature. SuperSIL lenses with NAs above 2 are possible with this design.

is coupled optically by means of a cryo-liquid that has a refractive index about that of water, does not boil at room temperature, and does not freeze at −140 °C, the temperature needed to keep vitreous ice from crystallizing. In this design, the warm objective necessarily delivers heat to the sample, which must be kept cold by removing the heat with a cold finger connected to the sample. The thermal conductance in the optical path must be such that the water layer is liquid while the sample is at ∼−140 °C. All this can and does happen over a fraction of a millimeter. Both implementations can be added to a commercial FM. In a different realization (Fig. 3*d*), one group used a super-hemispherical solid immersion lens (superSIL) with an NA of 2.17, which provides a potentially larger decrease in the root mean square (rms) error (Wang *et al.*, 2019). The superSIL lens, which is optically coupled to the cold sample and which operates at cryogenic temperatures, forms a virtual image of the sample below the plane of the sample. The virtual image is then magnified by a long working distance, low power objective operating at ambient temperature. This design can be added to a standard FM. We will consider later whether a higher NA aperture should be a goal.

There are fluorophores we can use for cryo-SMLM.

For a list of some FPs used for cryo-SMLM see Table 1 in Tuijtel *et al.* (2019) or Tables S1 and S2 in Hoffman *et al.* (2020). These two references also have accounts of how to do cryo-SMLM. For a complete listing of the properties of almost all FPs, see the FP Base (Lambert, 2019).

Of obvious interest is the number of photons each fluorophore emits on average before bleaching, which under cryogenic

https://doi.org/10.1017/S003358352100007X Published online by Cambridge University Press

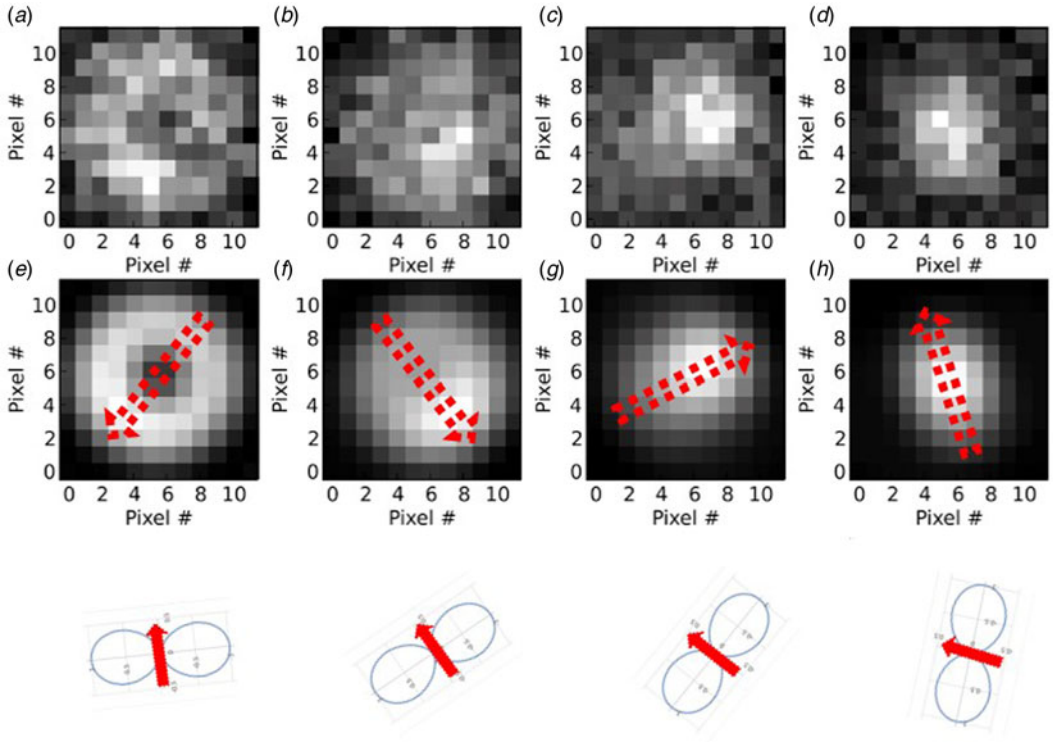

Fig. 4. The top row of images of the 2D PSF is actual micrographs of fluorophores with dipoles that are fixed in space. The second row shows the simulated images of the 2D PSF using the measured polar and azimuthal angles of the dipole as determined for the top row of images. The azimuthal angles of the dipoles are indicated by the red arrows in the second row of images. The arrowhead on the arrow indicates the direction of the lobe of the dipole's power profile closest to the objective. The third row shows the polar tilt of the dipole (indicated here by the red arrow) from the plane of the specimen. The lobes flanking the arrow show a cross section of the distribution of radiated power from the dipole. In the images, the true position of the fluorophore is the center of the image, which is at $x, y = 5, 5$. With each pixel being 44 nm, it is easy to see that a Gaussian fit to images in (c), for example, would result in a significant shift of the calculated peak position from the true position of the fluorophore. Reprinted with modification from Fig. 1 by permission from © Nature/Springer/Palgrave, *Nature Methods*, Mortensen *et al.* (2010).

conditions is significantly greater than that at ambient temperatures. As far as we know, all fluorophores fluoresce at cryo-temperatures, but not all are suitable for SMLM because they either must be switchable or they must blink appropriately. In a commercial cryo-FM (NA = 0.8) using Dronpa, a FP, about 2000 photons were detected before bleaching (Liu *et al.*, 2015), whereas for photoactivatable green fluorescent protein (PAGFP) with a NA = 1.2 objective, about 500 photons were detected before bleaching (Nahmani *et al.*, 2017). (Note that only a small percentage of photons emitted by a fluorophore is detected by microscopes.) Under cryo-conditions, PAmKate, another FP, may have the record yielding over 1 million detected photons before bleaching in one case, but this FP generally yields about 11 000 detected photons before bleaching. The resulting error in x, y localization of PAmKate was on average about 9 nm (Dahlberg *et al.*, 2018).

Capturing so many photons with the attendant decrease in errors may not be necessary and may cause another problem. PAmKate has such a long on-time that multiple molecules may fluoresce within the same diffraction limited volume (Dahlberg *et al.*, 2018) and/or the long lifetime may increase data collection time significantly. Moreover, given time constraints and the increased time to measure each fluorescent tag, fewer tags will be measured, which may be important depending on the project.

Indeed, in general, we must suspect that some of our 'events' captured on the detector will arise from two fluorescent sources emitting within the PSF at the same time even when the field of fluorophores is not crowded. If the two fluorophores are not too close together, their positions might be resolved using appropriate algorithms that test for such cases (Mailfert *et al.*, 2018). If they are too close together (well within the PSF), we can resolve them at least in principle, because they turn on and turn off or bleach independently (Gordon *et al.*, 2004). Let's assume that both are on at the same time when we start recording images. One will bleach or blink, and the image will dim and shift slightly from the absence of one signal. That shift can be used to determine the position of both fluorophores. A similar situation occurs if we start with one fluorophore on and another joins it within the PSF. The image will brighten and shift, and the positions can be determined from the shift. The problem that remains is that if we have very densely packed fluorophores, there may be too many to carry out SMLM.

Cryo-samples pose a particular problem.

We now return to the issue of the accuracy of the localization. In a frozen hydrated sample, we assume that the molecular dipoles are fixed in space and time. The distribution of photons emitted by the fluorophore depends on the azimuthal and polar angles of its dipole (Mortensen *et al.*, 2010) because the angular distribution of the emitted photons is not spherically symmetric but is doughnut-shaped with the 'hole' along the axis of the dipole. The PSF will not in general be symmetric much less Gaussian. Figure 4*a* to *h* illustrates the appearance of the PSFs found for

https://doi.org/10.1017/S003358352100007X Published online by Cambridge University Press

fixed dipoles at various angles. When the dipole is oriented perpendicular to the direction of view, there is no bias in the estimate of position of the fluorophore. We will return to this later. In the images, the center of the PSF is the middle pixel, and with each pixel corresponding to 44 nm, it is easy to see how a Gaussian fit could lead to errors in position. If we wish to determine the position accurately, we need to compare the observed distribution of photons to an array of theoretical distributions. This can be done, but it does add complexity to the instrumentation and/or analysis (Mortensen *et al.*, 2010; Backlund *et al.*, 2014). If we had assumed a Gaussian profile for the PSF, we would have systematic errors. The expected systematic errors *in focus* for a high NA objective (NA = 1.49) depend on the number of photons, varying from 10 nm with 500 photons to about 6 nm with 10 000 photons. With an objective having an NA <1, the deviation of the estimated and actual position of the fluorophore is negligible if the fluorophore is in focus and not too deep in the sample (Weisenburger *et al.*, 2014). There may be deviations from the true position, however, if the fluorophore is deep in the sample even if the image is in focus. Such errors might be only a few nanometers depending on the depth of the fluorophore. If the fluorophore is out of focus, however, and the dipole is tilted out of the plane normal to the optical axis, there will be deviations of the estimated position from the true position even with an NA <1. The errors grow quickly with defocus and can exceed 100 nm (Stallinga and Rieger, 2010; Engelhardt *et al.*, 2011; Backlund *et al.*, 2014). There is an optical trick for fixed dipoles that eliminates the bias in the localization. An azimuthally polarizing filter can ensure that the PSF appears axial so that there is no error in the position even with defocus (Lew and Moerner, 2014; Backlund *et al.*, 2016; Dahlberg and Moerner, 2021). In brief, the added optical element removes all but the radiation from the lateral component of the dipole so that all dipoles appear to be perpendicular to the axial direction and the bias is eliminated. The PSF, however, is elliptical laterally, and this will be a problem when determining the z position using astigmatic imaging. Moreover, there is a loss of photons, which undoes some of the advantage of the higher NA of the objective. There is room for more experimentation here.

Although we can collect more photons with a higher NA objective, we will require more complicated imaging and analysis to achieve the best resolution. With a lower NA objective, we will have a smaller error due to fixed dipoles but a larger error due to collecting fewer photons. One more thing: most laser excitation or switching light is plane polarized. Plane-polarized light maximally excites or switches fluorophores that have their dipoles parallel to the plane of polarization. If the plane of polarization is at right angles to the dipole, there is no excitation or switching. To excite or switch all fluorophores equally and independent of the orientation of their dipoles, we would have to use cross beam excitation (Valles and Hess, 2017), which may require higher NA objectives. At least we can use circularly polarized light in which the plane of polarized light rotates continuously. There are optical elements that convert plane to circularly polarized light, which will excite fluorophores with dipoles at any angle in the plane of the sample but less efficiently with dipoles tilted out of that plane. The problem is worse with lower NA objectives in which the angular spread of the excitation beam is smaller than with higher NA objectives.

Do fluorophores damage our target?

Does it matter if we do not capture as many photons as possible because we have a lower NA objective? It might because, sadly, fluorophores are not benign tags. As in the case of the miniSOG (Shu *et al.*, 2011), fluorophores generate destructive species such as free radicals, peroxides, etc. These agents may not only destroy the fluorophore, but may also damage or kill a cell. One such FP so readily destroys cells that it is aptly named killer red (Bulina, *et al.*, 2006). Of course, we would care about such damage if we were using fluorescent tags to mark the positions of targets that we want to subject to subtomogram averaging or if we have a high density of fluorophores in our region of interest. Such damage may be less important in other circumstances. In general, if we view the cell by fluorescence prior to freezing the cell, we should try to keep the power of the illuminating laser beams as low as possible and capture as many photons as possible to keep the cell in as near a native condition as possible.

When the cell is frozen, we get more photons before bleaching than we do at room temperature. The fluorophores still bleach, and the destructive species are still produced albeit at a greatly reduced rate due in part to the limited rate of oxygen diffusion under cryogenic conditions (Dahlberg and Moerner, 2021). Whether the number of reactive species is sufficient to damage a target is uncertain. But, if there are sufficient numbers, can these destructive species diffuse far enough to damage our target structure? There are some measurements of small molecules diffusing in amorphous ice. Diffusion characteristics of small molecules in low-density amorphous ice were modeled by molecular dynamics simulations and also measured experimentally (Ghesquière *et al.*, 2015). The diffusion coefficient of water molecules in vitreous ice at near liquid nitrogen temperatures varies from $\sim 10^{-14}$ to $10^{-15}\,\mathrm{cm}^2/\mathrm{s}$. The rms distance a molecule would travel is given by

$$\sqrt{\langle x^2 \rangle} = \sqrt{2Dt}$$

where D is the diffusion coefficient and t is the time. A water molecule could travel by diffusion about 1 nm in 1 s to about 8 nm in a minute. Given that we collect data over many minutes, we might want to determine experimentally if these destructive species can harm our target. Whatever we find, it is best to keep the sample as cold as possible and efficiently collect as many photons as possible consistent with the acceptable level of damage.

We must avoid melting our cryo-sample.

We have another consideration. Namely, a strong laser beam can heat the sample enough to cause the vitreous ice to become microcrystalline and compromise the quality of the cryo-EM images (Chang *et al.*, 2014). For very thin layers of ice, an intensity greater than $\sim 550\,\mathrm{W/cm}^2$ can cause such changes. This limited intensity increases the time needed to carry out the SMLM mapping of tags, which is not a good thing. Replacement of the layer of carbon on an EM grid, however, with a very thin layer of formvar, which is less absorbent of light than carbon, permits powers of $1.5\,\mathrm{kW/cm}^2$ (Liu *et al.*, 2015). It is not clear that the various literature measurements about acceptable laser powers are truly comparable. The maximum intensity may also depend on the heat conductivity of the cold stage, on the nature of the sample (Chang *et al.*, 2014), and on the wavelength used. We should, therefore, determine what power is acceptable given our lasers, cold stages, and our samples. The crystallization can be detected either by electron diffraction of the sample (e.g. Liu *et al.*, 2015) or by inspection of the images (Chang *et al.*, 2014).

https://doi.org/10.1017/S003358352100007X Published online by Cambridge University Press

What kind of cryo-FM do we need for cryo-CLEM?

The existing cryo-FMs may not be optimal. What features might we want in an improved cryo-FM for cryo-CLEM? To keep the design and data analysis as simple as possible while maintaining a reasonable accuracy, let 's consider a low NA, gas or vacuum coupled objective as in Fig. 3*a*. These cryo-stage designs, however, may not work for SMLM because the sample may distort the image of the fluorophore. The reason is that we want as little water left behind as possible when we blot the grid prior to freezing. This applies if we plan to look through the thinnest part of a cell such as a lamellipodium where a layer of ice would degrade the image. The same is true if we want to mill a lamella because we use the scanning electron microscope (SEM) image of the cell protruding above the grid to position the milling beam. The frozen cells sticking up from the grid into the cold gas or vacuum act as misshapen lenses that will distort the image of the fluorophore (Lauren Metskas, personal communication). Can we simply ignore the distortion? Suppose we want to look 5 µm deep into a cell using an NA = 0.8 objective. The diameter of the fluorescence exiting the cell surface that is collected by the objective is $d = 5 \times 2 \times \tan(\arcsin(0.8)) = 13$ µm. Thus, the surface of the cell should be flat to at least a quarter of a wavelength or about 125 nm over an area of about 13 by 13 µm^2. This constraint poses a particular problem for devices that combine cryo-FIB-SEM and cryo-FM. With the cells poking up into the vacuum, SMLM may require some modification.

The use of adaptive optics (Booth, 2014; Bonora *et al*., 2015), which tries to flatten the optical inhomogeneities, offers one avenue of approach to compensating for the protruding cell bodies, but such optics have not yet been used for this particular problem. We might be able to circumvent the problem by not looking down on top of the cell as it protrudes from the grid, but rather by using an inverted FM, we can look up through the flat side of the cell. This is the way cryo-SMLM was done by Chang *et al*. (2014). Another solution to the problem is to immerse the grid in an index matching cryo-fluid such as liquid propane ($n = 1.34$) or perhaps liquid ethane ($n = 1.38$) because the refractive index of the cytosol is about 1.35 (Hassani and Kreysing, 2019). Thus, we may want a cold stage in which the cells are sitting in a refractive-index-matching cryo-liquid. The cryo-FM designs in Fig. 3*b* or Fig. 3*c* would be a possibility. Remember that we must remove this cryo-liquid in order to carry out operations such as milling in the FIB-SEM or imaging in the EM. In one study, the cryo-fluid (a hydrocarbon) was removed from grids by washing in cold liquid ethane (Nahmani *et al*., 2017). Which cryo-liquid would be easiest to use while keeping localization errors in an acceptable range requires experimentation. The protrusion of cells from grids in an FIB-SEM device remains an issue to be solved and that applies to the commercially available cryo-stages on upright microscopes

To reduce the background as much as possible, we would like to use light-sheet illumination or something like it, if possible, so that we minimize background fluorescence from outside our zone of data collection. If we are considering what kind of cold stage we want, why not consider a built-in freezer? If propane or ethane is used as our cryo- liquid, we could design the stage so that the propane or ethane acts both as our cryogen and as our cryo-liquid. Thus, we could watch our cell while it is alive, blot and freeze it at the instant an event of interest has occurred, and map our fluorophore locations. Finally, we would remove the cryo-liquid and proceed to cryo-EM or cryo-FIB milling. Is this a device that will make our work easier? Can such a stage be produced? Is it just a matter of turning the engineering crank?

What are our localization goals for the cryo-FM and cryo-EM?

To determine the correct position to mill a 150 nm thick lamella, we need an error in z that is not much more than, let 's say, ~30 nm, which would help keep the target within the milled lamella on the one hand, and reduce the volume we might search to find the target on the other. Clearly, the choice of 30 nm is arbitrary and might be larger or smaller depending on the structure being studied. The error in z using a cylindrical lens at room temperature is about 20 nm (Huang *et al*., 2008), which is acceptable.

Whether the z position can be determined that accurately at cryo-temperatures using astigmatism remains to be determined given systematic errors from defocused images of fixed dipoles. Our other choice is to use a through focal series to determine the PSF in x, y, and z.

If we do not use an immersion objective, we must correct for the foreshortening of the depth of the fluorophore by the higher refractive index of the medium (e.g. cell cytoplasm) compared to the low refractive index of the air or vacuum. This foreshortening effect is seen when looking at a fish tank. The fish seem to be closer than they really are. Indeed, the true distance of the fluorophore from the refractive index boundary must be increased by multiplying the measured distance by the refractive index of the medium. The distance we measure in the FM is relative to the objective lens. We need to determine the z position relative to some position that can be used as reference in the milling machine or in our cryo-ET. If the support film on which the cells sit is fluorescently labeled, then we can use the change in focus from the support film to the tag in the cell to determine the actual depth (Fig. 5). We can probably ignore the effect of wavelength because the change in refractive index with wavelength, at least for water, is small ($\Delta n \sim 0.003$) over a range of 500–600 nm. The refractive index variation inside a cell, however, can vary from 1.355 to 1.390 (e.g. Zhang *et al*., 2017), which may lead to significant errors in determining z. If we have an SMLM microscope built into the FIB-SEM device, we could get an initial estimate of the tag's position, do a rough milling down to about 2 µm, and again determine the axial position. At a thickness of about 2 µm, an error in the refractive index will not cause a significant error in the position of the tag. At present, there are FIB-SEM instruments with an FM built in (Gorelick *et al*., 2019). Indeed, Delmic offers the Meteor, a commercially available inverted FM that can be added to an FIB-SEM. If the NA is about 0.90, it should be possible to adapt these FMs for SMLM. Moreover, having the mapping done in the FIB-SEM device reduces one interdevice transfer of the sample, which can reduce the possibility of ice contamination. There is now a better way to transfer samples, however, which may solve the transfer problem (Tacke *et al*., 2020). Clearly this is an area to be further explored.

If we can map the positions of fluorophores with tolerable errors, can we transfer those coordinates accurately from the cryo-FM to the cryo-FIB-SEM, which is used for milling lamellae, or to a cryo-ET? We will most likely need to make other measurements inside the FIB-SEM device or cryo-EM to align the SMLM map to the FIB-SEM or cryo-ET coordinate systems. A protocol exists for effecting a transfer from a cryo-FM to the cryo-EM (Schorb *et al*., 2017), but the accuracy, which is tens of nanometers, may not be sufficient for our purposes. The transfer will be

https://doi.org/10.1017/S003358352100007X Published online by Cambridge University Press

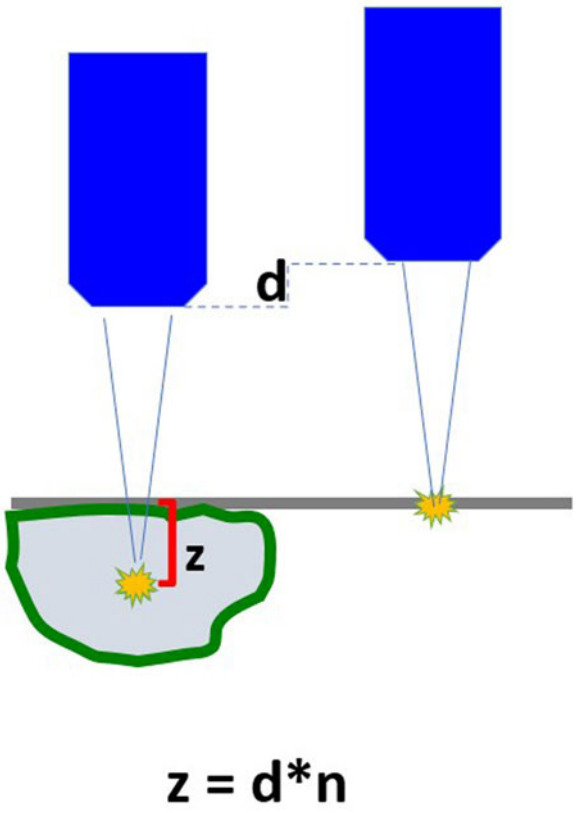

Fig. 5. The left side of the figure depicts an objective lens focused through a supporting film (horizontal blue line) onto a fluorophore (yellow burst) in the heart of a cell (dome-shaped structure) of refractive index *n*. The right side shows the objective focused on a fluorophore attached to the supporting film. The change in focus *d* multiplied by *n* gives the true position z of the fluorophore in the cell relative to the fluorophore on the grid.

much easier if an SMLM instrument is part of the FIB-SEM device, which will make the positioning of the milling beam much easier and may make the alignment of the fluorescent image to the ensuing cryo-ET of the milled lamella easier. This is an area that requires further work.

How well can we align the fluorescence map to the cryo-EM map?

We begin considering only *x*, *y* localization. In one study using a commercially available cryo-FM, Tuijtel *et al.* (2019) found that the mean error for localization of a tag was about 30 nm, and the mean error of alignment of the FM images to the EM images was also about 30 nm. The latter measurements were not made using fluorescent nanospheres but using fluorescent nanotubes aligned in projection. By combining the two sources of error with equal weights, we might expect the total error to be about 30 nm multiplied by the square root of 2, or about 50 nm. A direct measurement of the total error in superimposing fluorescent FM images with cryo-EM images was carried out (Schorb and Briggs, 2014). In this case, fluorescent beads were used to carry out the alignment of the FM and EM images. The targets in this case were fluorescent virus particles. The positions of the fluorescent images relative to the EM images of the virus particles revealed an average error of 50 nm. A part of the error was attributed to local distortions such as those caused by beam-induced motion (BIM) (Downing, 1991; Brilot *et al.*, 2012) in which the layer of ice over a hole in the grid becomes distorted when the electron beam is turned on.

With direct electron detectors (DEDs), we might be able to do better. DEDs are sensitive enough to divide a single exposure dose into a 'movie' of many frames. Corresponding regions of each frame could be aligned to one another and averaged to eliminate most of the BIM. Although the DEDs have thus enabled corrections for these motions (Campbell *et al.*, 2012), they are best done by local regions within an image rather than globally. The point is that the motions of fiducial markers can vary from one fiducial marker to the next, meaning that the positions of the fiducial markers can move relative to one another (Brilot *et al.*, 2012; Schorb and Briggs, 2014). Schorb and Briggs, who saw an average error of 50 nm, used a CCD camera, which provides a single image upon exposure of the specimen to the electron beam. Thus, these researchers would not have been able to make any correction for BIM. Given that we now have DEDs, we can take 'movies' instead of a single exposure, and we can do better. Since the initial frames in the movies are closest to the starting positions of the fiducials, seen in the FM, perhaps the use of the first frame as reference to align the other frames will keep the averaged EM image closest to that seen in the FM thus reducing the effect of BIM.

Fortunately for intact cells and FIB milled lamellae, BIM seems much smaller than in single particle cryo-EM. The additional bulk of cells keeps the BIM in some cases to 1–2 nm (Danielle Grotjahn, personal communication). Large organelles may also show limited BIM. At zero-degree tilt, there is essentially no BIM in images of cilia, whereas tilts of 30+ degrees can give rise to BIM of a few nanometers (Daniela Nicastro, personal communication). A method of using fiducials to correct for BIM in a tomographic series of images improves the alignment of images in the series to give better tomograms (Fernandez *et al.*, 2019). Every little bit helps.

Two recent papers have made efforts to locate fluorophores in cryo-EM maps. In the first paper (Dahlberg *et al.*, 2020), the authors aimed to locate the position of a particular protein in cryo-ETs of a thin bacterium. SMLM for a PAmKate tag with its high photon count gave a precision of about 9 nm on average in *x* and *y* and about 35 nm in *z*. The task of aligning the *x*, *y* positions of the fluorophores to the coordinate system of the tomogram was done in two steps. In the first step, fluorescence images were aligned to a low magnification electron micrograph using 12–16 holes in the EM grid. Next, 15–25 gold beads were used to align the low magnification EM image to an axial projection of the tomogram. This method was verified using tomograms of 40 nm fluorescent beads, and the authors determined an *x*, *y* registration error of ~30 nm. The axial registration proved problematic as expected with the suggestion that more investigation is needed. They were able to produce axial alignment by moving the grouping of fluorophore positions into a region of the cell previously known to contain the target proteins. Although fluorescent beads were used to check the accuracy of the method, they were not found to be the best features to use when aligning the SMLM map to the cryo-ET map.

The second paper (Hoffman *et al.*, 2020), which sets forth its methods in detail, superimposes the fluorescent tags onto an FIB-SEM map of a cell. The starting point is an SMLM map of a high-pressure frozen cell. The mapping was done through the sapphire disk on which the cells were frozen so that the issue of cells protruding into space was not a problem. The sample was

https://doi.org/10.1017/S003358352100007X Published online by Cambridge University Press

then subjected to freeze-substitution, heavy metal staining, FIB-SEM milling, and imaging. The registration of the SMLM map to the FIB-SEM map made use of intracellular organelles as fiducials. Because the various steps from freeze substitution to generating an FIB-SEM map introduced distortions, a non-linear mapping determined from the various fiducials was used to overlay the SMLM and FIB-SEM maps. The accuracy of the overlay in one example was 89 nm and in another 27 nm. The difference in accuracies may be attributable, for example, to the differences in the number of fiducials available or differences in the relative motions of the organelles during preparation and viewing but it was not due apparently to the precision of the localization of the tags. Perhaps we could design an FP with a distinctive shape that could be easily recognized in an EM map so we did not need such accurate alignments of SMLM maps to EM maps. As a community, we have more work to do to achieve localization for ever smaller structural targets.

Remember that what we localize is the tag not the target. We can use the position of the tag to define a local volume that should contain our target. At present, we can locate targets of known structure and sufficient size in 2D images (Rickgauer *et al.*, 2017). Can our SMLM (localization) map be of use in restricting the volumes within the tomogram that we need to search? Might not our SMLM map, by reducing the volume searched and hence the number of false positives, improve the sensitivity of the method? Might the SMLM map also be useful for localizing and determining the structure of a target whose structure is not known? Perhaps volumes around tags could be subjected to single particle methods to locate recurring structures within them. This is speculative, but we should keep it in mind.

Concluding remarks and outstanding questions

CLEM has been useful for many projects, but it has not yet been pushed to its limits. We have looked at the various problems associated in carrying out cryo-SMLM. There are paths to increasing the localization of tags and therefore targets, but we need more experimentation. We need to answer these and other questions:

(1) Do the destructive species generated by fluorescent tags attached to targets damage the targets?
(2) Do we want a cryo-FM equipped for SMLM as a stand-alone device perhaps with a built-in freeze plunger or do we want SMLM built into the FIB-SEM device?
(3) What is the best objective to use? Is a low NA objective, which is easier to use than a high NA objective good enough? If a higher NA objective is better, does an NA of 1.2 or 1.3 supply enough of an advantage to make it worthwhile? If an even higher NA is better, can we incorporate a superSIL objective to view a sample on an EM grid?
(4) What is the best way to measure *z*? Will one exposure with astigmatism or another trick work or do we need to take a through focal series?
(5) How can we best align our fluorescence map to our FIB-SEM image or to our cryo-ET?

Perhaps an international meeting to generate ideas is needed to decide which methods can best determine where in the cell is my protein.

Acknowledgements. I had valuable discussions with John Sedat (University of California, San Francisco), Dmitry Lyumkis (Salk Institute), Dorit Hanein and Niels Volkmann (Institut Pasteur and Scintillon Institute), Lauren Metskas (Cal Tech and Purdue), Danielle Grotjahn (Scripps Research, La Jolla), and her lab members (Ben Barad, Jess Rabuck-Gibbons, Ashim Rai, and Michaela Medina) and Keren Lasker (Stanford). I am also deeply indebted to Hari Schroff (National Institutes of Health) and Sam Hess (University of Maine) who introduced me to super-resolution light microscopy and helped me understand and design my first super-resolution microscope.

References

Adrian M, Dubochet J, Lepault J and McDowall AW (1984) Cryo-electron microscopy of viruses. *Nature* **308**, 32–36.

Backlund MP, Lew MD, Backer AS, Sahl SJ and Moerner WE (2014) The role of molecular dipole orientation in single-molecule fluorescence microscopy and implications for super-resolution imaging. *ChemPhysChem* **15**, 587–599.

Backlund MP, Arbabi A, Petrov PN, Arbabi E, Saurabh S, Faraon A and Moerner WE (2016) Removing orientation-induced localization biases in single-molecule microscopy using a broadband metasurface mask. *Nature Photonics* **10**, 459–462.

Bates M, Dempsey GT, Chen KH and Zhuang X (2012) Multicolor super-resolution fluorescence imaging via multi-parameter fluorophore detection. *ChemPhysChem* **13**, 99–107.

Baumeister W, Grimm R and Walz J (1999) Electron tomography of molecules and cells. *Trends in Cell Biology* **9**, 81–85.

Betzig E, Patterson GH, Sougrat R, Lindwasser OW, Olenych S, Bonifacino JS, Davidson MW, Lippincott- Schwartz J and Hess HF (2006) Imaging intracellular fluorescent proteins at nanometer resolution. *Science* **313**, 1642–1645.

Bohm J, Frangakis AS, Hegerl R, Nickell S, Typke D and Baumeister W (2000) Toward detecting and identifying macromolecules in a cellular context: template matching applied to electron tomograms. *Proceedings of the National Academy of Sciences of the United States of America* **97**, 14245–14250.

Bonora S, Jian Y, Zhang P, Zam A, Pugh EN, Zawadzki RJ and Sarunic MV (2015) Wavefront correction and high-resolution *in vivo* OCT imaging with an objective integrated multi-actuator adaptive lens. *Optics Express* **23**, 21931–21941.

Booth MJ (2014) Adaptive optical microscopy: the ongoing quest for a perfect image. *Light: Science & Applications* **3**, e165.

Brilot AF, Chen JZ, Cheng A, Pan J, Harrison SC, Potter CS, Carragher B, Henderson R and Grigorieff N (2012) Beam-induced motion of vitrified specimen on holey carbon film. *Journal of Structural Biology* **177**, 630–637.

Buckley G, Gervinskas G, Taveneau C, Venugopal H, Whisstock JC and de Marco A (2020) Automated cryo-lamella preparation for high-throughput in-situ structural biology. *Journal of Structural Biology* **210**, 107488.

Bulina ME, Chudakov DM, Britanova OV, Yanushevich YG, Staroverov DB, Chepurnykh TV, Merzlyak EM, Shkrob MA, Lukyanov S and Lukyanov KA (2006) A genetically encoded photosensitizer. *Nature Biotechnology* **24**, 95–99.

Campbell MG, Cheng A, Brilot AF, Moeller A, Lyumkis D, Veesler D, Pan J, Harrison SC, Potter CS, Carragher B and Grigorieff N (2012) Movies of ice-embedded particles enhance resolution in electron cryo-microscopy. *Structure* **20**, 1823–1828.

Chakraborty S, Jasnin M and Baumeister W. Three-dimensional organization of the cytoskeleton. (2020) A cryo-electron tomography perspective. *Protein Science* **29**, 1302–1320, Erratum in: Protein Sci. 29, 2132–2133.

Chang YW, Chen S, Tocheva EI, Treuner-Lange A, Löbach S, Søgaard-Andersen L and Jensen GJ (2014) Correlated cryogenic photoactivated localization microscopy and cryo-electron tomography. *Nature Methods* **11**, 737–739.

Chien FC, Lien CH and Dai YH (2015) Dual-color dynamic tracking of GM-CSF receptors/JAK2 kinases signaling activation using temporal focusing multiphoton fluorescence excitation and astigmatic imaging. *Optics Express* **23**, 30943–30955.

Dahlberg PD and Moerner WE (2021) Cryogenic super-resolution fluorescence and electron microscopy correlated at the nanoscale. *Annual Review of Physical Chemistry* **72**, 253–278.

https://doi.org/10.1017/S003358352100007X Published online by Cambridge University Press

Dahlberg PD, Sartor AM, Wang J, Saurabh S, Shapiro L and Moerner WE (2018) Identification of PAmKate as a red photoactivatable fluorescent protein for cryogenic super-resolution imaging. *Journal of the American Chemical Society* **140**, 12310–12313.

Dahlberg PD, Saurabh S, Sartor AM, Wang J, Mitchell PG, Chiu W, Shapiro L and Moerner WE (2020) Cryogenic single-molecule fluorescence annotations for electron tomography reveal *in situ* organization of key proteins in *Caulobacter*. *Proceedings of the National Academy of Sciences of the United States of America* **117**, 13937–13944.

Downing KH (1991) Spot-scan imaging in transmission electron microscopy. *Science (New York, N.Y.)* **251**, 53–59.

Engelhardt J, Keller J, Hoyer P, Reuss M, Staudt T and Hell SW (2011) Molecular orientation affects localization accuracy in superresolution far-field fluorescence microscopy. *Nano Letters* **11**, 209–213.

Faoro R, Bassu M, Mejia YX, Stephan T, Dudani N, Boeker C, Jakobs S and Burg TP (2018) Aberration- corrected cryoimmersion light microscopy. *Proceedings of the National Academy of Sciences of the United States of America* **115**, 1204–1209.

Fernandez JJ, Li S and Agard DA (2019) Consideration of sample motion in cryo-tomography based on alignment residual interpolation. *Journal of Structural Biology* **205**, 1–6.

Ghesquière P, Mineva T, Talbi D, Theulé P, Noble JA and Chiavassa T (2015) Diffusion of molecules in the bulk of a low density amorphous ice from molecular dynamics simulations. *Physical Chemistry Chemical Physics* **17**, 11455–11468.

Gordon MP, Ha T and Selvin PR (2004) Single-molecule high-resolution imaging with photobleaching. *Proceedings of the National Academy of Sciences of the United States of America* **101**, 6462–6465.

Gorelick S, Buckley G, Gervinskas G, Johnson TK, Handley A, Caggiano MP, Whisstock JC, Pocock R and de Marco A (2019) PIE-scope, integrated cryo-correlative light and FIB/SEM microscopy. *Elife* **8**, e45919.

Hassani H and Kreysing E (2019) Noninvasive measurement of the refractive index of cell organelles using surface plasmon resonance microscopy. *Optics Letters* **44**, 1359–1362.

Hess ST, Girirajan TP and Mason MD (2006) Ultra-high resolution imaging by fluorescence photoactivation localization microscopy. *Biophysical Journal* **91**, 4258–4272.

Hoffman DP, Shtengel G, Xu CS, Campbell KR, Freeman M, Wang L, Milkie DE, Pasolli HA, Iyer N, Bogovic JA, Stabley DR, Shirinifard A, Pang S, Peale D, Schaefer K, Pomp W, Chang CL, Lippincott-Schwartz J, Kirchhausen T, Solecki DJ, Betzig E and Hess HF (2020) Correlative three-dimensional super-resolution and block-face electron microscopy of whole vitreously frozen cells. *Science* **367**, eaaz5357.

Huang B, Wang W, Bates M and Zhuang X (2008) Three-dimensional super-resolution imaging by stochastic optical reconstruction microscopy. *Science* **319**, 810–813.

Juette MF, Gould TJ, Lessard MD, Mlodzianoski MJ, Nagpure BS, Bennett BT, Hess ST and Bewersdorf J (2008) Three-dimensional sub-100 nm resolution fluorescence microscopy of thick samples. *Nature Methods* **5**, 527–529.

Kao HP and Verkman AS (1994) Tracking of single fluorescent particles in three dimensions: use of cylindrical optics to encode particle position. *Biophysical Journal* **67**, 1291–1300.

Ke Z, Oton J, Qu K, Cortese M, Zila V, McKeane L, Nakane T, Zivanov J, Neufeldt CJ, Cerikan B, Lu JM, Peukes J, Xiong X, Kräusslich HG, Scheres SHW, Bartenschlager R and Briggs JAG (2020) Structures and distributions of SARS-CoV-2 spike proteins on intact virions. *Nature* **588**, 498–502.

Kühlbrandt W (2014) Biochemistry. The resolution revolution. *Science* **343**, 1443–1444.

Lambert TJ (2019) FPBase: a community-editable fluorescent protein database. *Nature Methods* **16**, 277–278.

Le Gros MA, McDermott G, Uchida M, Knoechel CG and Larabell CA (2009) High-aperture cryogenic light microscopy. *Journal of Microscopy* **235**, 1–8.

Lew MD and Moerner WE (2014) Azimuthal polarization filtering for accurate, precise, and robust single- molecule localization microscopy. *Nano Letters* **14**, 6407–6413.

Lew MD, Thompson MA, Badieirostami M and Moerner WE (2010) *In vivo* Three-Dimensional Superresolution Fluorescence Tracking using a Double-Helix Point Spread Function. 2010 Proc SPIE Int Soc Opt Eng. **7571**, 75710Z.

Li H and Vaughan JC (2018) Switchable fluorophores for single-molecule localization microscopy. *Chemical Reviews* **118**, 9412–9454.

Liu B, Xue Y, Zhao W, Chen Y, Fan C, Gu L, Zhang Y, Zhang X, Sun L, Huang X, Ding W, Sun F, Ji W and Xu T (2015) Three-dimensional super-resolution protein localization correlated with vitrified cellular context. *Scientific Reports* **5**, 13017–13028.

Mailfert S, Touvier J, Benyoussef L, Fabre R, Rabaoui A, Blache MC, Hamon Y, Brustlein S, Monneret S, Marguet D and Bertaux N (2018) A theoretical high-density nanoscopy study leads to the design of UNLOC, a parameter-free algorithm. *Biophysical Journal* **115**, 565–576.

Marko M, Hsieh C, Moberlychan W, Mannella CA and Frank J (2006) Focused ion beam milling of vitreous water: prospects for an alternative to cryo-ultramicrotomy of frozen-hydrated biological samples. *Journal of Microscopy* **222**, 42–47.

Marko M, Hsieh C, Schalek R, Frank J and Mannella C (2007) Focused-ion-beam thinning of frozen- hydrated biological specimens for cryo-electron microscopy. *Nature Methods* **4**, 215–217.

Metlagel Z, Krey JF, Song J, Swift MF, Tivol WJ, Dumont RA, Thai J, Chang A, Seifikar H, Volkmann N, Hanein D, Barr-Gillespie PG and Auer M (2019) Electron cryo-tomography of vestibular hair-cell stereocilia. *Journal of Structural Biology* **206**, 149–155.

Mortensen KI, Churchman LS, Spudich JA and Flyvbjerg H (2010) Optimized localization analysis for single-molecule tracking and super-resolution microscopy. *Nature Methods* **7**, 377–381.

Nahmani M, Lanahan C, DeRosier D and Turrigiano GG (2017) High-numerical-aperture cryogenic light microscopy for increased precision of superresolution reconstructions. *Proceedings of the National Academy of Sciences of the United States of America* **114**, 3832–3836.

Pennacchietti F, Gould TJ and Hess ST (2017) The role of probe photophysics in localization-based superresolution microscopy. *Biophysical Journal* **113**, 2037–2054.

Rickgauer JP, Grigorieff N and Denk W (2017) Single-protein detection in crowded molecular environments in cryo-EM images. *Elife* **6**, e25648.

Rigort A and Plitzko JM (2015) Cryo-focused-ion-beam applications in structural biology. *Archives of Biochemistry and Biophysics* **581**, 122–130.

Rust MJ, Bates M and Zhuang X (2006) Sub-diffraction-limit imaging by stochastic optical reconstruction microscopy (STORM). *Nature Methods* **3**, 793–795.

Sartori A, Gatz R, Beck F, Rigort A, Baumeister W and Plitzko JM (2007) Correlative microscopy: bridging the gap between fluorescence light microscopy and cryo-electron tomography. *Journal of Structural Biology* **160**, 135–145.

Schorb M and Briggs JA (2014) Correlated cryo-fluorescence and cryo-electron microscopy with high spatial precision and improved sensitivity. *Ultramicroscopy* **143**, 24–32.

Schorb M, Gaechter L, Avinoam O, Sieckmann F, Clarke M, Bebeacua C, Bykov YS, Sonnen AF, Lihl R and Briggs JAG (2017) New hardware and workflows for semi-automated correlative cryo-fluorescence and cryo-electron microscopy/tomography. *Journal of Structural Biology* **197**, 83–93.

Schur FK (2019) Toward high-resolution *in situ* structural biology with cryo-electron tomography and subtomogram averaging. *Current Opinion in Structural Biology* **58**, 1–9.

Schwartz CL, Sarbash VI, Ataullakhanov FI, McIntosh JR and Nicastro D (2007) Cryo-fluorescence microscopy facilitates correlations between light and cryo-electron microscopy and reduces the rate of photobleaching. *Journal of Microscopy* **227**, 98–109.

Shu X, Lev-Ram V, Deerinck TJ, Qi Y, Ramko EB, Davidson MW, Jin Y, Ellisman MH and Tsien RY (2011) A genetically encoded tag for correlated light and electron microscopy of intact cells, tissues, and organisms. *PLoS Biology* **9**, e1001041.

Siemons M, Cloin BMC, Salas DM, Nijenhuis W, Katrukha EA and Kapitein LC (2020) Comparing strategies for deep astigmatism-based single-molecule localization microscopy. *Biomedical Optics Express* **11**, 735–751.

Stallinga S and Rieger B (2010) Accuracy of the Gaussian point spread function model in 2D localization microscopy. *Optics Express* **18**, 24461–24476.

https://doi.org/10.1017/S003358352100007X Published online by Cambridge University Press

Tacke S, Erdmann P, Wang Z, Klumpe S, Grange M, Plitsko, J and Raunser S. (2020) A streamlined workflow for automated cryo focused ion beam milling. bioRxiv 2020.02.24.963033.

Thompson RE, Larson DR and Webb WW (2002) Precise nanometer localization analysis for individual fluorescent probes. *Biophysical Journal* **82**, 2775–2783.

Tuijtel MW, Koster AJ, Jakobs S, Faas FGA and Sharp TH (2019) Correlative cryo super-resolution light and electron microscopy on mammalian cells using fluorescent proteins. *Scientific Reports* **9**, 1369.

Valles M and Hess ST (2017) A cross beam excitation geometry for localization microscopy. *Isci Notes* **2017**, 1.

Wang L, Bateman B, Zanetti-Domingues LC, Moores AN, Astbury S, Spindloe C, Darrow MC, Romano M, Needham SR, Beis K, Rolfe DJ, Clarke DT and Martin-Fernandez ML (2019) Solid immersion microscopy images cells under cryogenic conditions with 12 nm resolution. *Communications Biology* **2**, 74.

Watanabe R, Buschauer R, Böhning J, Audagnotto M, Lasker K, Lu TW, Boassa D, Taylor S and Villa E (2020) The *in situ* structure of Parkinson's disease-linked LRRK2. *Cell* **182**, 1508–1518.

Weisenburger S, Jing B, Hänni D, Reymond L, Schuler B, Renn A and Sandoghdar V (2014) Cryogenic colocalization microscopy for nanometer-distance measurements. *ChemPhysChem* **15**, 763–770.

Weisenburger S, Boening D, Schomburg B, Giller K, Becker S, Griesinger C and Sandoghdar V (2017) Cryogenic optical localization provides 3D protein structure data with angstrom resolution. *Nature Methods* **14**, 141–144.

Zachs T, Schertel A, Medeiros J, Weiss GL, Hugener J, Matos J and Pilhofer M (2020) Fully automated, sequential focused ion beam milling for cryo-electron tomography. *Elife* **9**, e52286.

Zhang Q, Zhong L, Tang P, Yuan Y, Liu S, Tian J and Lu X (2017) Quantitative refractive index distribution of single cell by combining phase-shifting interferometry and AFM imaging. *Scientific Reports* **7**, 2532.

https://doi.org/10.1017/S003358352100007X Published online by Cambridge University Press